An error and stability analysis of four nonstationary wavefield extrapolators

Robert J. Ferguson and Gary F. Margrave

ABSTRACT

An error and stability analysis is presented for the elementary nonstationary wavefield extrapolators L_N^+, L_P^+ and their symmetric hybrids L_A^+ and L_{PN}^+. The analysis is based on analytic expressions that describe the inversion of wavefields extrapolated by the four operators. Our analysis shows that L_A^+ and L_{PN}^+ are more accurate and more stable than elementary extrapolators L_N^+ and L_P^+.

The Marmousi synthetic data is used to provide a comparison of depth imaging using the different extrapolators. The largest mean absolute amplitudes of the resulting depth images corresponding to L_N^+(~1000) and L_P^+(~1000) indicate that recursive application of these extrapolators caused growth in the extrapolated wavefield. The mean absolute amplitudes of L_A^+(~800) and L_{PN}^+(~800) were an order of magnitude less indicating greater stability. The best image of the model was returned by the L_A^+ method.

INTRODUCTION

Margrave and Ferguson (1999) present a comparison of four wavefield extrapolators that are useful in recursive explicit depth imaging methods. Two of them, L_N^+ and L_P^+ (NSPS and PSPI as introduced by Margrave and Ferguson (1997, 1999)), are derived from the Taylor series representation of extrapolated wavefields (Margrave and Ferguson (1999)). The remaining extrapolators, L_A^+ and L_{PN}^+, are formed by averaging (L_A^+) or cascading (L_{PN}^+) the elementary ones (L_N^+ and L_P^+).

Margrave and Ferguson (1999) demonstrate that, when velocity varies laterally, inversion of wavefields extrapolated by L_A^+ or L_{PN}^+ more closely return the input than do L_N^+ or L_P^+. Through analysis of the asymptotic formulae of the symbols of the depth derivatives corresponding to L_N^+ and L_P^+ they suggest that L_A^+ and L_{PN}^+ benefit from the averaging of these symbols. The symbols are complex valued and opposite in sign in the odd orders. Their average cancels these terms and returns a symbol that is real valued with error terms of higher order than the elementary symbols. The L_A^+ extrapolator averages the symbols at the Taylor series level through a summing of depth derivatives (Margrave and Ferguson, 1999). The L_{PN}^+ extrapolator may have the effect of averaging them through the cascade process (Margrave and Ferguson, 1999).

Margrave and Ferguson (1999) also demonstrate, by an analysis of the singular values of the extrapolators, that all four have some values larger than unity in the nonevanescent region. Thus, when used recursively, e.g., as in depth imaging they are prone to uncontrolled growth in the amplitude of the extrapolated wavefield, and extrapolation is unstable. Margrave and Ferguson (1999) find that L_A^+ and L_{PN}^+ have singular values closer to unity than L_N^+ and L_P^+, with L_A^+ being closest, suggesting that L_A^+ and L_{PN}^+ are more stable than the other two, and that L_A^+ is the most stable.

In this paper, wavefield extrapolators L_P^+, L_N^+, L_{PN}^+ and L_A^+ are evaluated for accuracy and stability by deriving the mathematical analogues of the inverse extrapolations presented by Margrave and Ferguson (1999). The resulting equations represent propagation from z = 0 to z through a laterally variable medium, followed by propagation from z back to z = 0. Assuming smooth variation of the extrapolation symbol α in lateral coordinate $\mathbf{x}$ we prove that L_{PN}^+ and L_A^+ are invertable and that inversion of L_P^+ and L_N^+ results in complex valued error terms.

The Marmousi synthetic data set (Bourgeois et al., 1990) is used to compare the accuracy and stability of depth imaging methods based on the different extrapolators.

INVERSE OPERATORS, ACCURACY AND STABILITY

Inversion of a wavefield ψ extrapolated by L_P^+ has an associated error that results in an approximation ψ_P to ψ given by

$$\psi_P(\mathbf{x}) = \left[L_P^- \int \left[L_P^+ \varphi(\mathbf{m})\right](\mathbf{y}) \exp(i\mathbf{k}\cdot\mathbf{y}) d\mathbf{y}\right](\mathbf{x}) \quad , \tag{1}$$

where,

$$\left[L_P^+ \varphi(\mathbf{m})\right](\mathbf{y}) = \frac{1}{(2\pi)^2} \int \alpha(\mathbf{y},\mathbf{m}) \varphi(\mathbf{m}) \exp(-i\mathbf{y}\cdot\mathbf{m}) d\mathbf{m} \quad , \tag{2}$$

and the symbol of this pseudo-differential operator is

$$\alpha(\mathbf{y},\mathbf{m}) = \exp\left(iz\sqrt{\left(\frac{\omega}{c(\mathbf{x})}\right)^2 - \mathbf{k}\cdot\mathbf{k}} \right). \tag{3}$$

Depth z is the extrapolation depth interval, ω is temporal frequency and $c(\mathbf{x})$ is the laterally variant velocity of the medium. Coordinates $\mathbf{x} = \{x_1, x_2\}$ correspond to output space, $\mathbf{y} = \{y_1, y_2\}$ correspond to input space, $\mathbf{m} = \{m_1, m_2\}$ correspond to input wavenumbers, $\mathbf{k} = \{k_1, k_2\}$ correspond to output wavenumbers. The spectrum of the wavefield is φ. The sign on z controls the direction of propagation (Margrave and Ferguson, 1999).

Equation (1) is the composition of two *pseudo-differential* operators L_P^+ (z positive) and L_P^- (z negative) that results in an equivalent operator L_P with the form

$$\psi_P(\mathbf{x}) = [L_P \varphi(\mathbf{m})](\mathbf{x}) \quad , \tag{4}$$

In integral form, equation (4) is

$$[L_P \varphi(\mathbf{m})](\mathbf{x}) = \frac{1}{(2\pi)^2} \int c_P(\mathbf{x},\mathbf{m}) \varphi(\mathbf{m}) \exp(-i\mathbf{m}\cdot\mathbf{x}) d\mathbf{m} \quad , \tag{5}$$

with symbol c_P given by

$$c_P(\mathbf{x},\mathbf{m}) = \frac{1}{(2\pi)^2} \iint \alpha^-(\mathbf{x},\mathbf{k}) \alpha^+(\mathbf{y},\mathbf{m}) \exp(-i[\mathbf{k}-\mathbf{m}]\cdot[\mathbf{x}-\mathbf{y}]) d\mathbf{y} d\mathbf{k} \quad . \tag{6}$$

Because inversion symbol c_P equation (6) results from the composition of two pseudo-differential operators it has an asymptotic formula (Stein, 1993: 237)

$$c_P(\mathbf{x},\mathbf{m}) = 1 + i\nabla_\mathbf{m}\alpha^-(\mathbf{x},\mathbf{m})\cdot\nabla_\mathbf{x}\alpha^+(\mathbf{x},\mathbf{m}) + \frac{i^2}{2}\nabla_\mathbf{m}\nabla_\mathbf{m}\alpha^-(\mathbf{x},\mathbf{m}) \mathbf{:} \nabla_\mathbf{x}\nabla_\mathbf{x}\alpha^+(\mathbf{x},\mathbf{m}) + \cdots \quad , \tag{7}$$

where $\nabla_\mathbf{m}$ and $\nabla_\mathbf{x}$ are gradient operators, and the **:** operator represents the contraction of two-second rank tensors. Symbol c_P is unity in the first term, and all other terms represent error, with odd powers being complex valued. For α constant in $\mathbf{x}$, c_P *is* unity and L_P, equation (5), reduces to an inverse Fourier transform. (Inversion is exact for constant velocity.)

Inversion of L_N^+ applied to ψ results in an approximation φ_N to spectrum φ given by

$$\varphi_N(\mathbf{m}) = \left[L_N^- \frac{1}{(2\pi)^2} \int [L_N^+ \psi(\mathbf{x})](\mathbf{k}) \exp(-i\mathbf{k}\cdot\mathbf{y}) d\mathbf{k} \right](\mathbf{m}) \quad , \tag{8}$$

where,

$$[L_N^\pm \psi(\mathbf{x},)](\mathbf{k}) = \int \alpha(\mathbf{x},\mathbf{k}) \psi(\mathbf{x}) \exp(i\mathbf{k}\cdot\mathbf{x}) d\mathbf{x} \quad . \tag{9}$$

Equation (8) is a composition of two *adjoint-standard* pseudo-differential operators L_N^+ and L_N^-, whose equivalent operator L_N has the form

$$\varphi_N(\mathbf{m}) = [L_N \psi(\mathbf{x})](\mathbf{m}) \quad , \tag{10}$$

or as an integral

$$[L_N \psi(\mathbf{x})](\mathbf{m}) = \int c_N(\mathbf{x},\mathbf{m})\psi(\mathbf{x})\exp(i\mathbf{m}\cdot\mathbf{x})d\mathbf{x} , \tag{11}$$

with symbol c_N

$$c_N(\mathbf{x},\mathbf{m}) = \frac{1}{(2\pi)^2}\iint \alpha^-(\mathbf{y},\mathbf{m})\alpha^+(\mathbf{x},\mathbf{k})\exp(-i[\mathbf{m}-\mathbf{k}]\cdot[\mathbf{x}-\mathbf{y}])d\mathbf{y}d\mathbf{k} . \tag{12}$$

Like c_P, inversion symbol c_N is the composition of two pseudo-differential operators, and it too has an asymptotic formula (Appendix A)

$$c_N(\mathbf{x},\mathbf{m}) = 1 - i\nabla_{\mathbf{m}}\alpha^-(\mathbf{x},\mathbf{m})\cdot\nabla_{\mathbf{x}}\alpha^+(\mathbf{x},\mathbf{m}) + \frac{i^2}{2}\nabla_{\mathbf{m}}\nabla_{\mathbf{m}}\alpha^-(\mathbf{x},\mathbf{m}):\nabla_{\mathbf{x}}\nabla_{\mathbf{x}}\alpha^+(\mathbf{x},\mathbf{m}) - \cdots . \tag{13}$$

Symbol c_N is similar to c_P (equation (7)); the first term is unity and the error terms are products of derivatives. However, the odd powers of derivatives in differ in sign. This suggests that an average of c_N and c_P will cancel complex values and increase the order of the error of the resulting symbol. In the limit of constant velocity, equation (11) reduces to a Fourier transform.

In the space domain, the inversion of the average operator L_A^+ is

$$[L_A \psi(\mathbf{y})](\mathbf{x}) = [L_A^- L_A^+ \psi(\mathbf{y})](\mathbf{x}) , \tag{14}$$

where from Margrave and Ferguson (1999)

$$[L_A^+ \psi(\mathbf{y})](\mathbf{x}) = \frac{1}{2}[L_N^+ \psi(\mathbf{y})](\mathbf{x}) + \frac{1}{2}[L_P^+ \psi(\mathbf{y})](\mathbf{x}) . \tag{15}$$

Expansion of equation (14), by replacing L_A^+ and L_A^- gives

$$[L_A \psi(\mathbf{y})](\mathbf{x}) = \frac{[L_P \psi(\mathbf{y})](\mathbf{x})}{4} + \frac{[L_N \psi(\mathbf{y})](\mathbf{x})}{4} + \frac{[L_P^- L_N^+ \psi(\mathbf{y})](\mathbf{x})}{4} + \frac{[L_N^- L_P^+ \psi(\mathbf{y})](\mathbf{x})}{4} . \tag{16}$$

The first two terms of L_A consist of the inversion operators L_P and L_N cast in the space domain as

$$[L_P \psi(\mathbf{y})](\mathbf{x}) = \int \psi(\mathbf{y})\frac{1}{(2\pi)^2}\int c_P(\mathbf{x},\mathbf{k})\exp(-i\mathbf{k}\cdot[\mathbf{x}-\mathbf{y}])d\mathbf{k}d\mathbf{y} , \tag{17}$$

and

$$[L_N\psi(\mathbf{y})](\mathbf{x}) = \int \psi(\mathbf{y}) \frac{1}{(2\pi)^2} \int c_N(\mathbf{y},\mathbf{k}) \exp(-i\mathbf{k}\cdot[\mathbf{x}-\mathbf{y}]) d\mathbf{k} d\mathbf{y} \quad . \tag{18}$$

L_P and L_N are transposes in this domain. Substitution of c_P equation (7) and c_N equation (1) in equations (17) and (18) gives for L_P

$$[L_P\psi(\mathbf{y})](\mathbf{x}) =$$
$$\psi(\mathbf{x}) + i\int \frac{1}{(2\pi)^2} \int \psi(\mathbf{x}) \nabla_\mathbf{k}\alpha(\mathbf{x},\mathbf{k}) \cdot \nabla_\mathbf{x}\alpha(\mathbf{x},\mathbf{k}) \exp(-i\mathbf{k}\cdot[\mathbf{x}-\mathbf{y}]) d\mathbf{k} d\mathbf{y} + i^2 \cdots , \tag{19}$$

and for L_N

$$[L_N\psi(\mathbf{y})](\mathbf{x}) =$$
$$\psi(\mathbf{x}) - i\int \frac{1}{(2\pi)^2} \int \psi(\mathbf{y}) \nabla_\mathbf{k}\alpha(\mathbf{y},\mathbf{k}) \cdot \nabla_\mathbf{y}\alpha(\mathbf{y},\mathbf{k}) \exp(-i\mathbf{k}\cdot[\mathbf{x}-\mathbf{y}]) d\mathbf{k} d\mathbf{y} + i^2 \cdots . \tag{20}$$

Operators L_P, and L_N differ only in the sign of the odd orders of their derivatives (the odd orders are also complex). Their sum cancels these terms and increases the order of the error terms giving for the first two terms in equation (16)

$$\frac{[L_P\psi(\mathbf{y})](\mathbf{x})}{4} + \frac{[L_N\psi(\mathbf{y})](\mathbf{x})}{4} = \frac{\psi(\mathbf{x})}{2}$$
$$+\frac{1}{2} i^2 \int \frac{1}{(2\pi)^2} \int \psi(\mathbf{y}) \nabla_\mathbf{k}\nabla_\mathbf{k}\alpha(\mathbf{y}) : \nabla_\mathbf{y}\nabla_\mathbf{y}\alpha(\mathbf{y}) \exp(-i\mathbf{k}\cdot[\mathbf{x}-\mathbf{y}]) d\mathbf{k} d\mathbf{y} + \cdots \tag{21}$$

The third term in equation (16) corresponds to forward extrapolation by L_N^+ followed by reverse extrapolation by L_P^-

$$[L_P^- L_N^+ \psi(\mathbf{y})](\mathbf{x}) = \int \psi(\mathbf{y}) \frac{1}{(2\pi)^2} \int \alpha^-(\mathbf{x},\mathbf{k}) \alpha^+(\mathbf{y},\mathbf{k}) \exp(-i\mathbf{k}\cdot[\mathbf{x}-\mathbf{y}]) d\mathbf{k} d\mathbf{y} \quad . \tag{22}$$

Substituting $\mathbf{u} = \mathbf{x} - \mathbf{y}$ in equation (22) gives

$$[L_P^- L_N^+ \psi(\mathbf{y})](\mathbf{x}) = \int \psi(\mathbf{x}-\mathbf{u}) \frac{1}{(2\pi)^2} \int \alpha^-(\mathbf{x},\mathbf{k}) \alpha^+(\mathbf{x}-\mathbf{u},\mathbf{k}) \exp(-i\mathbf{k}\cdot\mathbf{u}) d\mathbf{k} d\mathbf{u} \quad . \tag{23}$$

Wavefield ψ can be approximated by Taylor series

$$\psi(\mathbf{x}-\mathbf{u}) = \psi(\mathbf{x}) - \mathbf{u}\cdot\nabla_\mathbf{x}\psi(\mathbf{x}) + (-\mathbf{u}\cdot\nabla_\mathbf{x})^2\psi(\mathbf{x}) - \cdots \quad . \tag{24}$$

Similarly, symbol α^+

$$\alpha^+(\mathbf{x}-\mathbf{u},\mathbf{k}) = \alpha^+(\mathbf{x},\mathbf{k}) - \mathbf{u}\cdot\nabla_\mathbf{x}\alpha^+(\mathbf{x},\mathbf{k}) + (-\mathbf{u}\cdot\nabla_\mathbf{x})^2\alpha^+(\mathbf{x},\mathbf{k}) - \cdots \quad . \tag{25}$$

Replacing ψ and α^+ in equation (23) with equations (24) and (25) gives

$$\left[L_P^- L_N^+ \psi(\mathbf{y})\right](\mathbf{x}) \ = \\ \int \left\{ [1 - \mathbf{u}\cdot\nabla_{\mathbf{x}} + \cdots]\psi(\mathbf{x}) \right\} \frac{1}{(2\pi)^2} \int \alpha^-(\mathbf{x},\mathbf{k}) \left\{ [1 - \mathbf{u}\cdot\nabla_{\mathbf{x}} + \cdots]\alpha^+(\mathbf{x},\mathbf{k}) \right\} \exp(-\mathbf{k}\cdot\mathbf{u}) d\mathbf{k} d\mathbf{u} \,. \tag{26}$$

The first order terms in equation (26) are, beginning with the simplest

$$\begin{aligned} &\psi(\mathbf{x}) \int \frac{1}{(2\pi)^2} \int \alpha^-(\mathbf{x},\mathbf{k}) \alpha^+(\mathbf{x},\mathbf{k}) \exp(-\mathbf{k}\cdot\mathbf{u}) d\mathbf{k} d\mathbf{u} \\ &= \psi(\mathbf{x}) \end{aligned} \,, \tag{27}$$

next,

$$\begin{aligned} &\nabla_{\mathbf{x}}\psi(\mathbf{x}) \cdot \int \mathbf{u} \frac{1}{(2\pi)^2} \int \alpha^-(\mathbf{x},\mathbf{k}) \alpha^+(\mathbf{x},\mathbf{k}) \exp(-\mathbf{k}\cdot\mathbf{u}) d\mathbf{k} d\mathbf{u} \\ &= \nabla_{\mathbf{x}}\psi(\mathbf{x}) \cdot \int \frac{1}{(2\pi)^2} \int \mathbf{u} \exp(-\mathbf{k}\cdot\mathbf{u}) d\mathbf{u} d\mathbf{k} \\ &= 0 \end{aligned} \,. \tag{28}$$

and,

$$\begin{aligned} &\psi(\mathbf{x}) \int \alpha^-(\mathbf{x},\mathbf{k}) \nabla_{\mathbf{x}} \alpha^+(\mathbf{x},\mathbf{k}) \cdot \frac{1}{(2\pi)^2} \int \mathbf{u} \exp(-\mathbf{k}\cdot\mathbf{u}) d\mathbf{u} d\mathbf{k} \\ &= \psi(\mathbf{x}) \int \alpha^-(\mathbf{x},\mathbf{k}) \nabla_{\mathbf{x}} \alpha^+(\mathbf{x},\mathbf{k}) \delta(\mathbf{k}) d\mathbf{k} \\ &= \psi(\mathbf{x}) \left\{ \nabla_{\mathbf{k}} \alpha^-(\mathbf{x},\mathbf{k}) \nabla_{\mathbf{x}} \alpha^+(\mathbf{x},\mathbf{k}) + \alpha^-(\mathbf{x},\mathbf{k}) \nabla_{\mathbf{x}} \nabla_{\mathbf{k}} \alpha^+(\mathbf{x},\mathbf{k}) \right\}_{\mathbf{k}=0} \\ &= 0 \end{aligned} \,, \tag{29}$$

where for this last term,

$$\begin{aligned} &\nabla_{\mathbf{k}} \alpha^\pm(\mathbf{x},\mathbf{k})_{\mathbf{k}=0} = \pm\left[z\alpha^\pm(\mathbf{x},\mathbf{k}) k_z(\mathbf{x},\mathbf{k}) \nabla_{\mathbf{k}} k_z(\mathbf{x},\mathbf{k}) \right]_{\mathbf{k}=0} \\ &= 0 \end{aligned} \,, \tag{30}$$

and

$$\begin{aligned} &\nabla_{\mathbf{k}} k_z(\mathbf{x},\mathbf{k})_{\mathbf{k}=0} = \left[\frac{1}{2} \left[\left(\frac{\omega}{c(\mathbf{x})} \right)^2 + \mathbf{k}\cdot\mathbf{k} \right]^{-\frac{1}{2}} \mathbf{k} \right]_{\mathbf{k}=0} \\ &= 0 \end{aligned} \,. \tag{31}$$

Assuming that second order terms (and higher) are small, equation (26) reduces to the identity

$$\left[L_P^- L_N^+ \psi(\mathbf{y})\right](\mathbf{x}) \approx \psi(\mathbf{x}) \quad , \tag{32}$$

from which we infer, to first order, L_P^- and L_N^+ are approximate inverses and, therefore, the fourth term in equation (16) is

$$\left[L_N^- L_P^+ \psi(\mathbf{y})\right](\mathbf{x}) \approx \psi(\mathbf{x}) \quad . \tag{33}$$

The inversion operator L_A, equation (16), is now written to first order as

$$\left[L_A \psi(\mathbf{y})\right](\mathbf{x}) \approx \psi(\mathbf{x}) \quad . \tag{34}$$

The results from the previous discussion are sufficient to derive the inversion of L_{PN}^+

$$\left[L_{PN} \psi(\mathbf{y})\right](\mathbf{x}) = \left[L_P^{-\frac{1}{2}} L_N^{-\frac{1}{2}} L_P^{\frac{1}{2}} L_N^{\frac{1}{2}} \psi(\mathbf{y})\right](\mathbf{x}) \quad , \tag{35}$$

and, using the associative properties of these operators, to first order L_P^- and L_N^+ are inverses, therefore

$$\left[L_{PN} \psi(\mathbf{y})\right](\mathbf{x}) \approx \psi(\mathbf{x}) \quad . \tag{36}$$

For comparison, L_P (equation (19)) to first order, is

$$\begin{aligned}&\left[L_P \psi(\mathbf{y})\right](\mathbf{x}) \approx \\ &\psi(\mathbf{x}) + i\int \frac{1}{(2\pi)^2} \int \psi(\mathbf{x}) \nabla_{\mathbf{k}} \alpha(\mathbf{x},\mathbf{k}) \cdot \nabla_{\mathbf{x}} \alpha(\mathbf{x},\mathbf{k}) \exp(-i\mathbf{k} \cdot [\mathbf{x}-\mathbf{y}]) d\mathbf{k} d\mathbf{y} \quad ,\end{aligned} \tag{37}$$

and for L_N

$$\begin{aligned}&\left[L_N \psi(\mathbf{y})\right](\mathbf{x}) \approx \\ &\psi(\mathbf{x}) - i\int \frac{1}{(2\pi)^2} \int \psi(\mathbf{y}) \nabla_{\mathbf{k}} \alpha(\mathbf{y},\mathbf{k}) \cdot \nabla_{\mathbf{y}} \alpha(\mathbf{y},\mathbf{k}) \exp(-i\mathbf{k} \cdot [\mathbf{x}-\mathbf{y}]) d\mathbf{k} d\mathbf{y} \quad .\end{aligned} \tag{38}$$

Inverses L_{PN} (equation (36)) and L_A (equation (34)) have no first order error terms. Inverse operators L_P (equation (37)) and L_N (equation (38)) have first order error terms that are functions of spatial and wavenumber derivatives that are non zero for smooth variation in velocity. Thus, in this situation, extrapolators L_{PN}^+ and L_A^+ are more accurate than L_P^+ and L_N^+.

In terms of stability, again to first order, L_P and L_N have complex error terms, suggesting that L_P^+ and L_N^+ also generate complex values. Uncontrolled complex values during recursive application of these extrapolators may lead to the instability observed by Margrave and Ferguson (1999).

MARMOUSI

The Marmousi synthetic data (Bourgeois et al., 1990) were acquired for use in comparing depth imaging methods based on extrapolators L_N^+, L_P^+, L_A^+ and L_{PN}^+. The prestack data were depth imaged at a depth interval of 20m. This interval was chosen as being large enough to illustrate the different stability and accuracy characteristics of the extrapolators without becoming unstable enough to preclude comparison. For a detailed description of prestack depth imaging using nonstationary extrapolators see Ferguson and Margrave (1999).

Figure 1 shows the true reflectivity computed from the density and velocity profile of the model. Figures 2 through 5 show the depth images corresponding to L_N^+ (Figure 2), L_P^+ (Figure 3), L_A^+ (Figure 4) and L_{PN}^+ (Figure 5). The depth-imaging algorithm based on L_A^+ gives the best image, especially in the shallower part of the model. (Arrows annotated on the figures facilitate this comparison.) The steeply dipping faults are more clearly imaged using L_A^+, and a large part of the section is less obscured by noise.

Comparison of the average amplitudes of the images of Figure 2 through 5 show that L_A^+ and L_{PN}^+ are more stable than L_N^+ and L_P^+. The average absolute amplitudes corresponding to L_A^+ (~800) and L_{PN}^+ (~800) are 20% less than those corresponding to L_N^+ (~1000) and L_P^+ (~1000).

CONCULSIONS

An error and stability analysis was presented for the nonstationary wavefield extrapolators L_N^+, L_P^+, L_A^+ and L_{PN}^+ defined by Margrave and Ferguson (1999) based on analytic expressions that describe inversion of wavefields extrapolated by the four operators. The analysis supports the conclusions of Margrave and Ferguson (1999) that L_A^+ and L_{PN}^+ are more accurate and more stable than elementary extrapolators L_N^+ and L_P^+. The first order result (i.e., smooth variation of the extrapolation symbol α in lateral coordinate $\mathbf{x}$) proved the error related to the inversion of L_{PN}^+ and L_A^+ is less than the inversion of L_P^+ and L_N^+. Similarly, the greater stability of L_{PN}^+ and L_A^+ was indicated.

The Marmousi model data (Bourgeois et al., 1990) were used to provide a qualitative comparison of depth imaging methods based on the different extrapolators. The best image of the model was returned by the L_A^+ method. Comparison of the average amplitudes of the images showed that the depth images for all four extrapolators had grown in amplitude but that L^+_{PN} and L^+_A had grown 20% less than L^+_P and L^+_N.

ACKNOWLEDGEMENTS

For his technical assistance, the authors thank Michael Loughlean of Alberta Energy Company (AEC) Ltd. We also thank the sponsors of CREWES for their support of this research.

REFERENCES

Bourgeois, A., Bourget, M., Lailly, P., Poulet, M., Ricarte, P., and Versteeg, R., 1990, Marmousi, model and data: in The Marmousi experience, EAGE, 5 - 9.

Ferguson R. J., and Margrave G. F., 1999, Prestack depth migration by symmetric nonstationary phase shift: CREWES Research Report, **11**, *This issue.*

Margrave, G. F. and Ferguson, R. J., 1997, Wavefield extrapolation by nonstationary phase shift: 67th Annual Internat. Mtg., Soc. Expl. Geophys., Expanded Abstracts, 1599-1602.

Margrave, G. F. and Ferguson, R. J., 1999, Taylor series derivation of nonstationary wavefield extrapolators: CREWES Research Report, **11**, *This issue*.

Stein, E. M., 1993, Harmonic analysis: real-variable methods, orthogonality, and oscillatory integrals: Princeton University Press.

APPENDIX A

Computing the spatial Fourier transform in c_N equation (12) gives

$$c_N(\mathbf{x},\mathbf{m}) = \frac{1}{(2\pi)^2}\int A^-(\mathbf{m}-\mathbf{k},\mathbf{m})\alpha^+(\mathbf{x},\mathbf{k})\exp(-i[\mathbf{m}-\mathbf{k}]\cdot\mathbf{x})d\mathbf{k} \quad . \tag{A1}$$

Equation (A1) can also be written

$$c_N(\mathbf{x},\mathbf{m}) = \frac{1}{(2\pi)^2}\int A^-(\mathbf{u},\mathbf{m})\alpha^+(\mathbf{x},\mathbf{m}-\mathbf{u})\exp(-i\mathbf{u}\cdot\mathbf{x})d\mathbf{u} \quad . \tag{A2}$$

Expanding α^+ results in

$$c_N(\mathbf{x},\mathbf{m}) = \frac{1}{(2\pi)^2}\int A^-(\mathbf{u},\mathbf{m})\left[\alpha^+(\mathbf{x},\mathbf{m}) - \mathbf{u}\cdot\nabla_{\mathbf{m}}\alpha^+(\mathbf{x},\mathbf{m}) + \cdots\right]\exp(-i\mathbf{u}\cdot\mathbf{x})d\mathbf{u} \quad , \tag{A3}$$

that provides an asymptotic formula for c_N that is similar to that of c_P by recognizing that coordinates **u** arise as spatial derivatives of the Fourier kernal thus

$$c_N(\mathbf{x},\mathbf{m}) = 1 - i\nabla_{\mathbf{m}}\alpha^-(\mathbf{x},\mathbf{m})\nabla_{\mathbf{x}}\alpha^+(\mathbf{x},\mathbf{m}) + \frac{i^2}{2}\nabla^2_{\mathbf{m}}\alpha^-(\mathbf{x},\mathbf{m}) : \nabla^2_{\mathbf{x}}\alpha^+(\mathbf{x},\mathbf{m}) - \cdots \quad . \tag{A4}$$

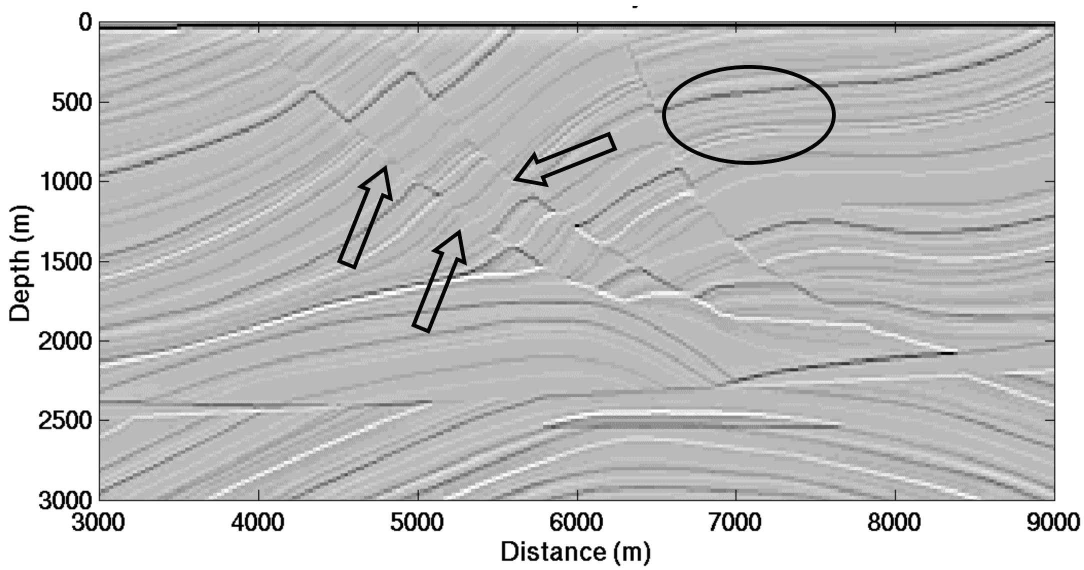

Fig. 1. The seismic reflectivity of Marmousi computed from the density and velocity profile of the model. The arrows and ring correspond to points of comparison with Figures 2 through 5.

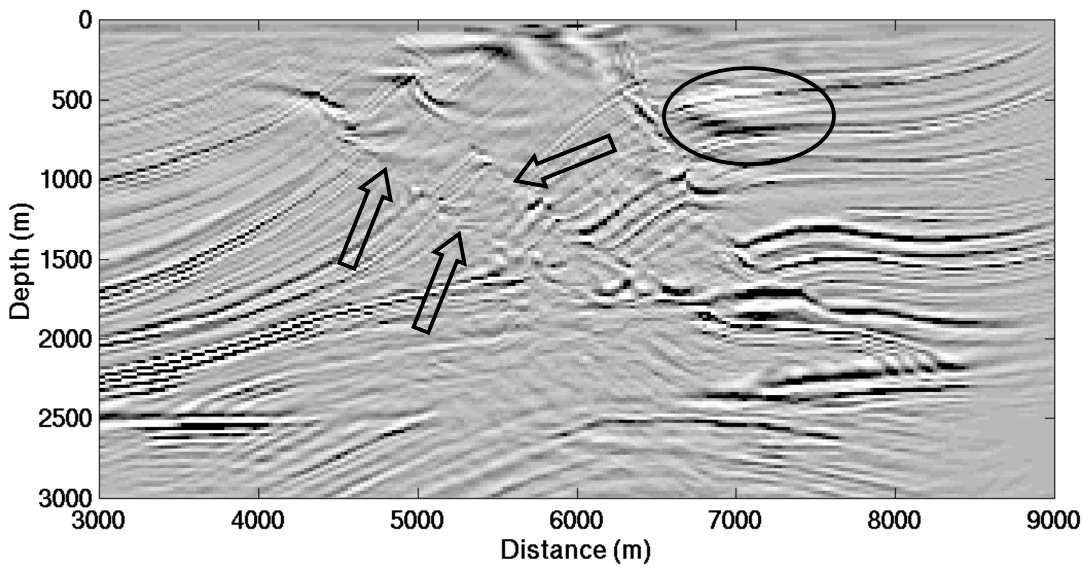

Fig. 2. Depth image of the Marmousi data set corresponding to L_N^+. The depth interval was 20m. The mean absolute amplitude of this image is ~1000. The arrows indicate points of comparison on two faults in the model. The ring encloses a flatter region that seems to suffer from noise. In this image the noise corresponds to a trough followed by a peak.

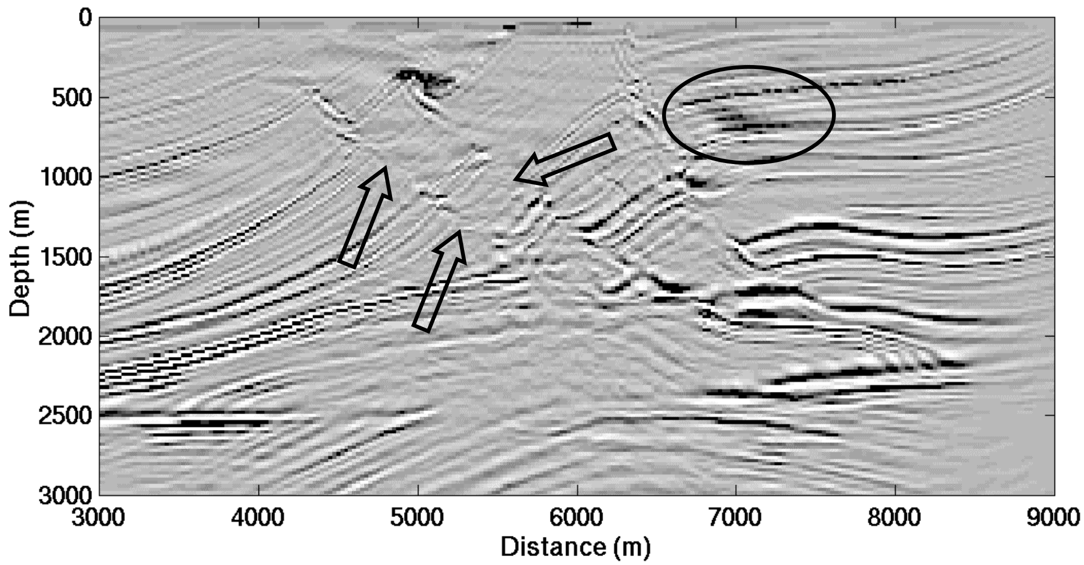

Fig. 3. Depth image of the Marmousi data set corresponding to L_P^+. The depth interval was 20m. The mean absolute amplitude of this image is ~1000. The images of the indicated faults are less well rendered by L_P^+ compared to L_A^+ (Figure 3). The noise in the ringed area is a strong peak.

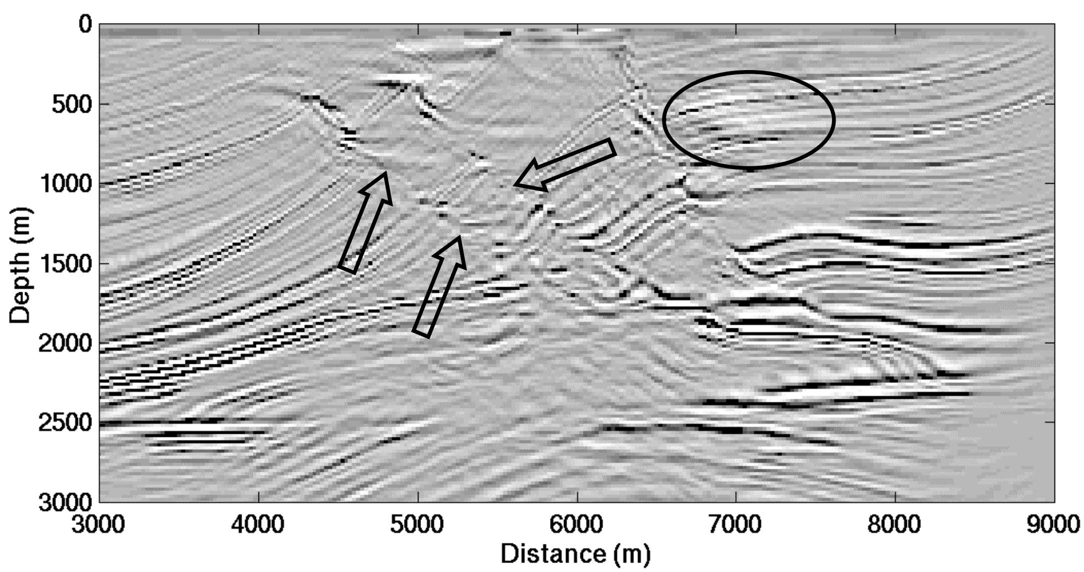

Fig. 4. Depth image of the Marmousi data set corresponding to L_A^+. The depth interval was 20m. The mean absolute amplitude of this image is ~800. The best focussing of the indicated faults is provided by this image. The noise in the ringed area is a strong trough.

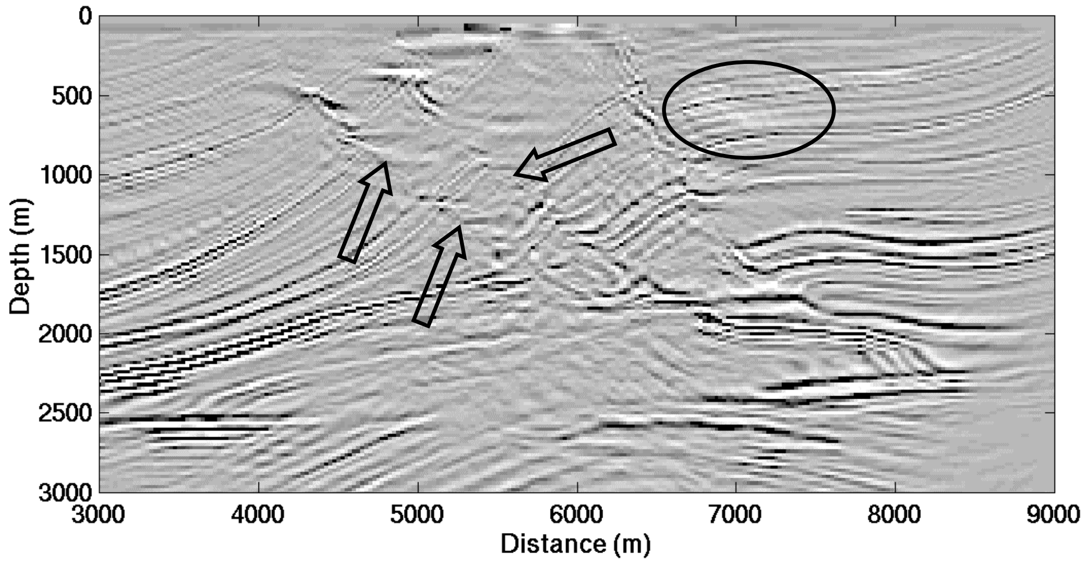

Fig. 5. Depth image of the Marmousi data set corresponding to L^{+}_{PN}. The depth interval was 20m. The mean absolute amplitude of this image is ~800. This image has the lowest noise in the ringed area.